minerals

Article

Investigation of Particle Motion in a Dry Separation Fluidized Bed Using PEPT

Meng Zhou [1], Ozan Kökkılıç [1], Darryel Boucher [1], Mark Lepage [1], Thomas W. Leadbeater [2,3], Raymond Langlois [1] and Kristian E. Waters [1,*]

1 Department of Mining and Materials Engineering, McGill University, MH Wong Building, 3610 University, Montreal, QC H3A 0C5, Canada
2 School of Physics and Astronomy, University of Birmingham, Edgbaston, Birmingham B15 2T8, UK
3 Department of Physics, University of Cape Town, P. Bag, Rondebosch 7701, South Africa
* Correspondence: kristian.waters@mcgill.ca; Tel.: +1-514-398-4492

Abstract: Developing dry separation methods to replace the commonly used water-based separation has become crucial due to increasing water shortages. One of the candidates for dry processing is gas–solid fluidized beds. The bed behavior and solid motion in fluidized beds have been investigated using various visual and numerical methods for decades. However, there are not enough studies focused on the separation behavior of the fine particles. This work details the investigation of particle motion through a fluidized bed using the positron emission particle tracking (PEPT) technique. Single-particle tracking is a powerful mechanism providing knowledge about separation mechanisms through direct visualization of the particle trajectory determined from recording the particle position over time. In this study, the movements of different-sized beds were characterized by tracking an activated single quartz particle and then by tracking an activated single hematite particle. The separation behavior of a heavy particle was determined for different-sized fractions.

Keywords: fluidized bed; gravity concentration; particle motion; positron emission particle tracking (PEPT)

check for updates

Citation: Zhou, M.; Kökkılıç, O.; Boucher, D.; Lepage, M.; Leadbeater, T.W.; Langlois, R.; Waters, K.E. Investigation of Particle Motion in a Dry Separation Fluidized Bed Using PEPT. *Minerals* **2023**, *13*, 254. https://doi.org/10.3390/min13020254

Academic Editor: Thomas Mütze

Received: 25 January 2023
Accepted: 8 February 2023
Published: 11 February 2023

1. Introduction

Water shortage has become a worldwide problem [1–4]. As many mining areas are located in cold, arid, or water-scarce regions, such as Canada, Australia, Chile, India, South Africa, and China, developing dry separation methods to replace commonly used water-based techniques has become more and more important [5–10]. In addition, because of the enormous amounts of water being used, wet processes require wastewater treatment and water recovery processes such as filters, centrifuges, and thickeners, which increase the capital and operating costs. Dry processes have been applied in various ore beneficiations, such as coal [11–21], iron [22–26], copper [27,28], and tungsten [29,30], as well as solid waste separation [31–36], to solve these problems associated with treatment and storage of wastewater. Even though the separation efficiency of dry processing is considered lower than wet processing, the overall economic benefits of dry processing are becoming increasingly relevant [16,17,19,22,24–26].

Apart from being concerned with water issues, mineral processing plants consume around 5% of the generated global electricity annually. Approximately 80% of this would be spent in the comminution units [37]. The development of more energy efficient and dry comminution technologies has been an important focus of academia and industry. Novel technologies, such as high-pressure grinding rolls (HPGR) and conjugate anvil hammer mill (CAHM), are designed and developed to fulfil the goal. Their potential to improve energy efficiency in the comminution process as dry grinding alternatives to replace conventional crushers and semi-autogenous grinding (SAG) mills has been indicated [38–40]. As mineral deposits are becoming increasingly more finely disseminated, and water scarcity has become a global issue, investigation of dry separation in fine sizes is of great importance.

One of the candidates for dry processing is gas–solid fluidized beds. Fluidized bed technology has been used since the 1920s. Due to its features such as excellent heat transfer, ease of solid handling, ease of particle processing and efficient solid mixing, it has been widely used in the chemical and petrochemical, energy, environmental, pharmaceutical, food processing, and biochemical industries [41–43]. The various applications of fluidized beds are the gasification and combustion of coal [44,45], ash separation and carbon capture [46,47], fluid catalytic cracking, Fischer–Tropsch synthesis, drying [48,49], cooling, heat transfer [50,51], size enlargement, size reduction, coating [52,53], solid mixing [54], mass transfer [55], fuel cleaning [56], and classification [41,42,57,58].

Fluidization is a process in which a fluid, either a gas or a liquid, passes through a packed bed of solid particles at a velocity that is sufficient to lift the particles. These lifted beds of solid particles obtain fluidlike properties such as apparent density and viscosity, and because of these properties, the fluidized particles can be used as the dense separation media [25,41,57]. There are two major types of separation in gas–solid fluidized systems, which are float–sink and segregation. When objects enter a fluidized bed, a float–sink process occurs; objects with lower density than the apparent density of the fluidized bed float, while objects with larger density sink into the fluidized bed. Moreover, controlling the apparent density of the fluidized bed, by changing the air velocity for fluidization or the density of the solid bed with mixing two types of particles with different densities, makes the separation of objects with different densities possible [25,32,59]. When a mixture of particles is fluidized, a segregation process occurs; heavier and/or larger particles start to move to the bottom, while lighter and/or smaller particles start to move to the top of the fluidized bed. Based on the density or size differences, the process is termed as density segregation or size segregation, respectively [16,60,61].

Previous research has investigated the behavior of bed and solid motion in fluidized beds using various techniques, including: optical probes [62], the laser sheet system [63], high-speed cameras [64], digital image analysis [54]; particle tracking velocimetry [49,65], radioactive particle tracking (RPT) [66], and numerical methods such as computational fluid dynamics (CFD) [45,67,68], the discrete element method (DEM) [69–71], and other numerical and mathematical models [27,43,72,73]. Dry separation technologies are increasingly being used, especially in China's coal preparation, covering a limited size range down to about 0.5 mm [74]. However, for dense minerals such as iron ore, separations are limited to particles larger than 11 mm [24]. There are relatively few studies that have focused on the separation behavior of fine particles (<0.5 mm). For these reasons, this research focused on the investigation of bed and fine particle motions to gain better understanding of possible fine particle separation in a gas–solid fluidized bed. Moreover, the visual systems have their own limitations for investigating opaque media, mixtures with high particle concentrations, or non-transparent systems. Positron emission particle tracking (PEPT) has allowed investigations of such systems.

PEPT was designed to study particle dynamics, granular systems, and multiphase flows with localizing a single traceable particle labeled with a positron-emitting radionuclide. This technique was developed at the University of Birmingham, UK [75,76] and has been described in detail by Leadbeater et al. [77,78]. The main advantage of PEPT over other techniques is that it allows the recording of a tracer particle motion inside dense, opaque systems and through solid vessel walls, allowing the detailed study [78] and tracking of a tracer particle over a long period of time. This enables the estimation of the behavior of particles and can provide useful information about particle motion [79]. PEPT has been employed for a variety of equipment such as fluidized beds [52,80–88], stirred [89,90] and tumbling mills [91–93], stirred tanks [94], mechanically agitated vessels [95–97], hydrocyclones [98–100], spiral concentrators [101,102], and flotation cells [103–111].

The ADAC Forte positron camera at the University of Birmingham Positron Imaging Centre, Birmingham, UK, was used to investigate bed movement using positron emission particle tracking. The bulk bed material was fine quartz and was represented using an activated quartz tracer particle, with an activated hematite particle representing the heavy phase.

2. Materials and Methods

2.1. Materials

Mono-sized (−300 + 212, −212 + 150, −150 + 106 µm) fine quartz (Unimin Canada Ltd., Havelock, ON, Canada), which is a typical Geldart Group B solid (40 µm < d_{particle} < 500 µm, 4 g/cm^3 > ρ_{particle} > 1.4 g/cm^3) [43,112–114], was used as the fluidized bed medium, and single-sized (−300 + 212, −212 + 150, −150 + 106 µm) fine hematite (Gem and Mineral Miners Inc., Alta Loma, CA, USA) was used as a heavy material subjected to gravity separation experiments. Single-sized quartz was used to avoid size effects on bed movement and separation.

2.2. Fluidized Bed and PEPT Setup

The fluidized bed consisted of a bed body, an air chamber, an air distributor, and a flow meter attached to the air chamber to measure the airflow for minimum fluidization and to adjust the desired air ratio for experiments. The bed body was made of a cylindrical transparent Plexiglas column with an inner diameter of 100 mm and height of 900 mm, and for the air distributor, a quartz frit (Technical Glass Products, QPD100-0) covered with a 38 µm screen sheet was used. In order to measure the change in bed height over time, the sidewall of the bed was marked with a graduated scale.

PEPT analysis was carried out using the ADAC Forte positron camera [115]. Large (−1180 + 1000 µm) quartz and hematite (ArcelorMittal Exploitation Minière, Longueuil, QC, Canada) particles were irradiated with a 35 MeV ^{3}He beam in the Birmingham MC40 cyclotron to produce the positron-emitting isotope ^{18}F in situ in the material matrix. These oxygen-containing minerals are well-suited for direct activation. An independent activation run was performed for each test. These large particles were broken after activation using a brass hammer and anvil and then were sized to the desired diameter using standard screens. The technique of producing tracer particles for PEPT work has been described in detail [99,101–103,116]. The fluidized bed set-up was placed inside the field of the camera, as shown in Figure 1.

The column was filled to a height of 300 mm to create a bed with mono-sized silica. Air was introduced to fluidize the bed from the bottom. The airflow rate for minimum fluidization (u_{mf}) was measured by increasing the airflow rate from 0 L/min to a certain rate where the bed expanded and bubbling occurred, which indicated the minimum fluidization of the Geldart Group B type particle [112,113]. With the addition of hematite, preliminary observations showed that the segregation of heavy and light particles did not occur under the minimum fluidization. For separation purposes, the airflow rate was set as 25% and 50% more than the minimum fluidization, and these conditions were used for all PEPT investigations.

The desired airflow rates and corresponding u_{mf} values used during the experiments for different-sized beds are given in Table 1. The bed was fluidized for a certain time (approximately 10 min) to reach an initial state with desired airflow depending on the experimental conditions. After that, the quartz tracer or the hematite tracer (mixed with 300 g hematite for separation purposes) was added to the top of the bed in each case for the investigation of the bed movement experiments or for separation-behavior experiments, respectively. Data recorded by the acquisition system were analyzed using the Track program [76,78], and post-treated with a customized MATLAB code. Track, developed at the University of Birmingham, is used to identify and reject corrupt events and to determine the location of the tracer particle [76]. An analysis of the raw data, obtained from the fluidized bed tests, is needed to determine optimum input parameters for the Track code for each corresponding speed and tracer activity level in order to minimize the 3D location error. This trajectory error analysis has been described in detail previously [99].

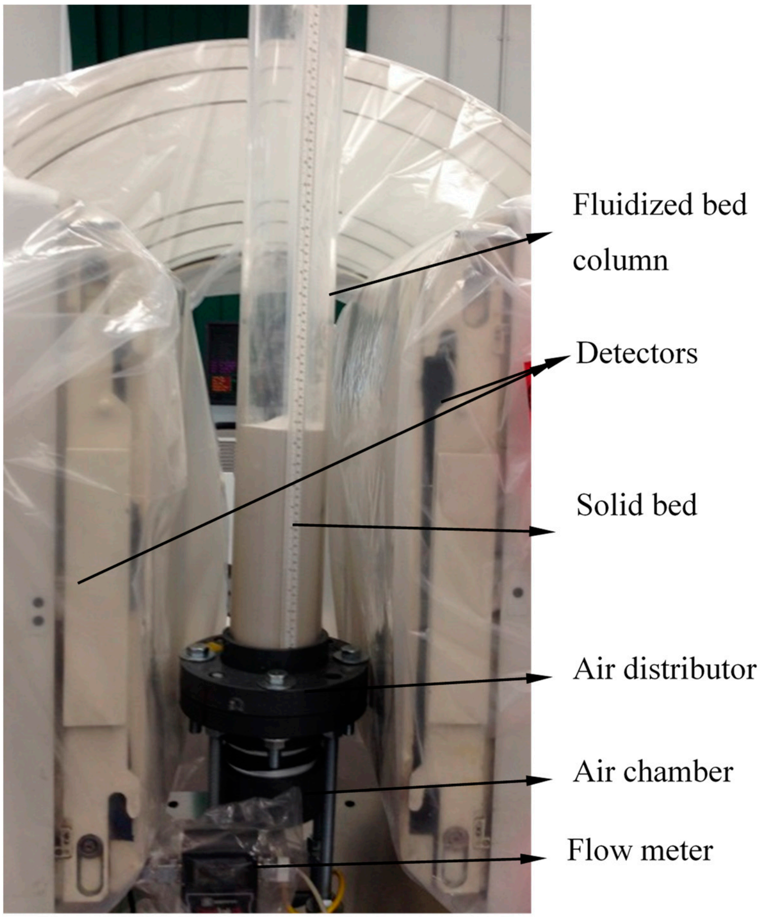

Figure 1. ADAC Forte positron camera with the fluidized bed placed between the detectors.

Table 1. Airflow rates for different stages.

Bed Size (µm)	Airflow (L/min)	u_{mf} (cm/s)	Airflow (L/min)	1.25 u_{mf} (cm/s)	Airflow (L/min)	1.5 u_{mf} (cm/s)
−300 + 212	33	7.00	41.25	8.75	49.5	10.50
−212 + 150	22	4.67	27.5	5.84	33	7.00
−150 + 106	16	3.40	20	4.24	24	5.09

3. Results and Discussion

3.1. Investigation of the Bed

A series of experiments were carried out to investigate the motion of the fluidized bed by tracking activated quartz particles (tracer) with airflow rates of 1.25 and 1.5 u_{mf} for each size fraction. Figure 2 presents vertical velocities of the activated quartz particle in each fluidized bed at different airflow rates, which demonstrates particle motions inside the beds. The trajectories of the tracer particle during the entire experimental run can be seen from Appendix A, Figures A1–A3 for each size fraction.

In the bed of size −300 + 212 µm, despite the airflow rate differences, the flow patterns look similar to deeper beds [41]. As can be seen from Figure 2a,b, both beds show the particle ascending at the center and descending near the wall [80]. The absolute velocity of the descending particle on the walls is relatively low (<0.01 m/s) for both airflow rates. However, the ascending particles in the center move faster than the corresponding downwards motion and the ascending region is slightly expanded at a high airflow rate (1.5 u_{mf}). The effect of the ascending particle will be discussed in the separation Section 3.2.1.

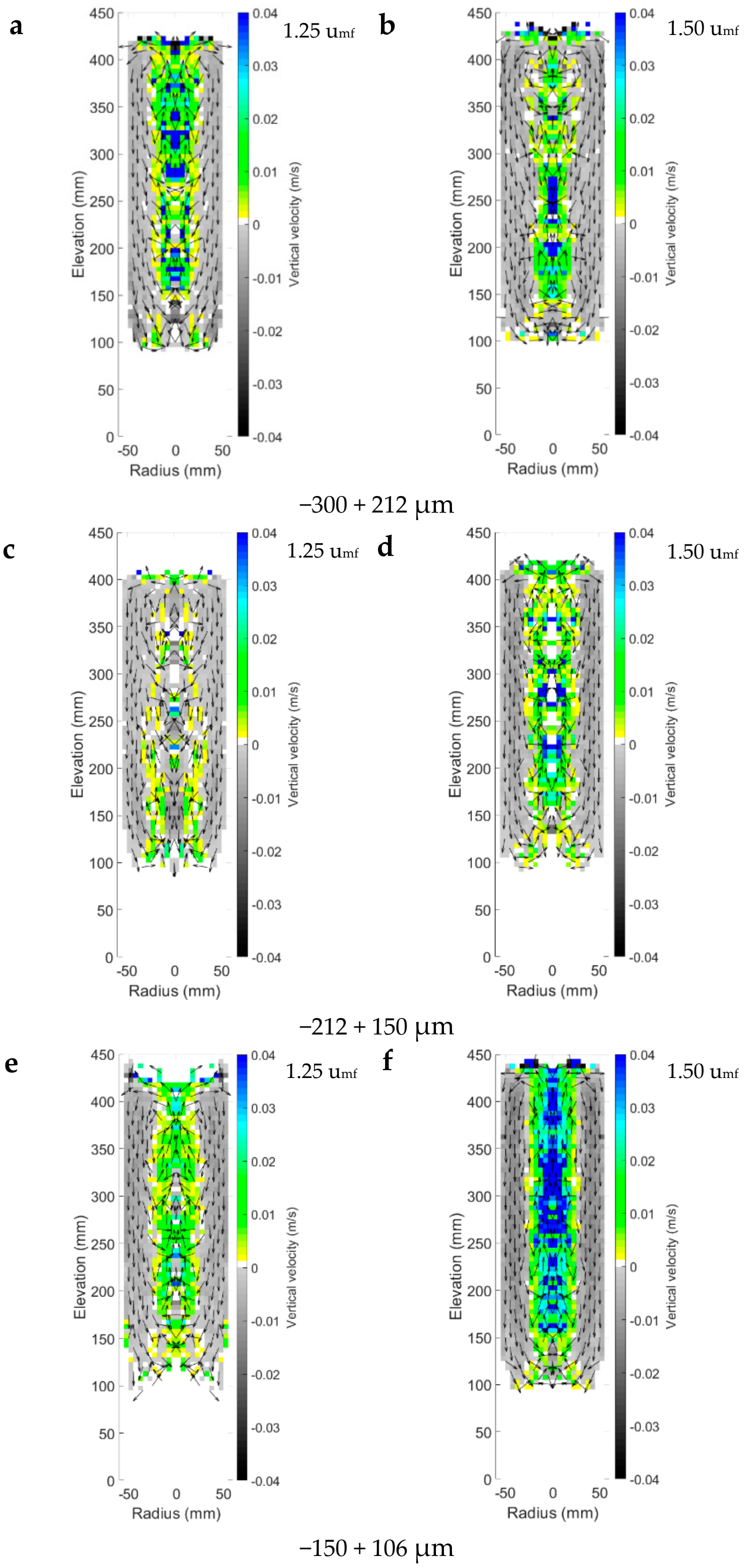

Figure 2. Vertical velocities of the activated quartz particle in each fluidized bed for an airflow rate of 1.25 u_{mf} (**left column**) and 1.50 u_{mf} (**right column**) for decreasing particle size (**top** to **bottom**). (**a**) −300 + 212 μm at 1.25 u_{mf}; (**b**) −300 + 212 μm at 1.50 u_{mf}; (**c**) −212 + 150 μm at 1.25 u_{mf}; (**d**) −212 + 150 μm at 1.50 u_{mf}; (**e**) −150 + 106 μm at 1.25 u_{mf}; (**f**) −150 + 106 μm at 1.50 u_{mf}.

Different to the coarser-sized bed (−300 + 212 μm), Figure 2c shows that, at a lower airflow rate (1.25 u_{mf}), the −212 + 150 μm bed starts to descend in the center and ascend between the center and the wall. However, according to Figure 2d, under a higher airflow rate (1.5 u_{mf}) the flow pattern of the bed looks similar to the −300 + 212 μm bed with the particle ascending at the center and descending near the wall. The flow pattern for this condition looks similar, but the absolute velocity of the ascending and descending particle is faster (>0.01 and > 0.015 m/s, respectively) than the coarser bed (−300 + 212 μm).

As for the −150 + 106 μm fluidized bed, based on Figure 2e, it shows that the overall bulk motion is still similar to the −212 + 150 μm bed (1.25 u_{mf}), but the speed distribution is higher. The particle descends near the wall and ascends in the center. However, there is a descending region in the middle when the figure is investigated closely. From Figure 2f, the flow patterns of the solids under higher airflow rate behave similarly to the −300 + 212 μm bed for both airflow rates and the −212 + 150 μm bed at the 1.25 u_{mf} bed, where the particle ascends at the center and descends near the wall. However, the absolute velocity of the ascending and descending particle is faster (>0.015 and >0.02 m/s, respectively), and the ascending particle reaches the maximum velocity (0.04 m/s) at the top half of the column center.

3.2. Separation Behavior and Heavy-Particle Motion

Experiments were conducted to investigate the movement of an activated heavy hematite particle in the same-sized fluidized bed with two airflow rates, 1.25 and 1.50 u_{mf}, respectively. Each size fraction was tested twice with different activated hematite particles. An additional test was added for the −300 + 212 μm fraction at both airflow rates due to promising separation.

3.2.1. The −300 + 212 μm Hematite Bed

Figures 3 and 4 show the results of the three runs (a, b, and c) for the −300 + 212 μm hematite particle with an airflow rate of 1.25 u_{mf} and 1.50 u_{mf}, respectively.

As seen from the Figure 3(a1,b1,c1), all heavy particles reach the bottom of the bed in a relatively short time (approximately 5 min) at an airflow rate of 1.25 u_{mf}. Investigating the route of the heavy particle shows that it follows the descending bed movement near the walls (Figure 3(a2,a3,b2,b3,c2,c3)). The absolute velocity of the particle shows that the heavy particle moves faster than the descended bed velocity, possibly due to the combined effects of bed movement and gravity.

The same behaviors were observed for the airflow rate of 1.5 u_{mf} (Figure 4(a1,a2,a3,b1, b2,b3)) apart from the last run (Figure 4(c1,c2,c3)). As mentioned in Section 3.1, the ascended bed velocity and its region is slightly bigger at an airflow rate of 1.50 u_{mf}. It is clear that there are one or more convective cells present in the bed at different heights, and there may be more cells as the airflow rate increases. Thus, there is more chance for the heavy particle to become entrained in a local convection cell. This explains why the heavy particle remained in the middle of the fluidized bed for a period of time before moving downward. However, heavy particles in this size (−300 + 212 μm) could still overcome the impact from the bulk ascending bed motion and eventually reached the bottom of the bed. Results from the third run indicate that a higher airflow rate leads to a longer separation time.

The heavy particles shown in Figure 5(a1,b1) do not remain at the bottom of the bed during the two runs. In both cases, the particle descends first in the descended bed region, and as soon as it reaches the center of the bed, it starts to ascend with the airflow and the rest of the bed (Figure 5(a2,a3,b2,b3)). During the first run (Figure 5(a1)), the particle reaches just the middle of the bed. One of the reasons for this behavior is the high absolute velocity of the ascended region, which pushes the particle upward in the center more easily. However, the tracer particle cannot stay in the middle of the bed during the second run (Figure 5(b1)) and it reaches the bottom of the bed in the end.

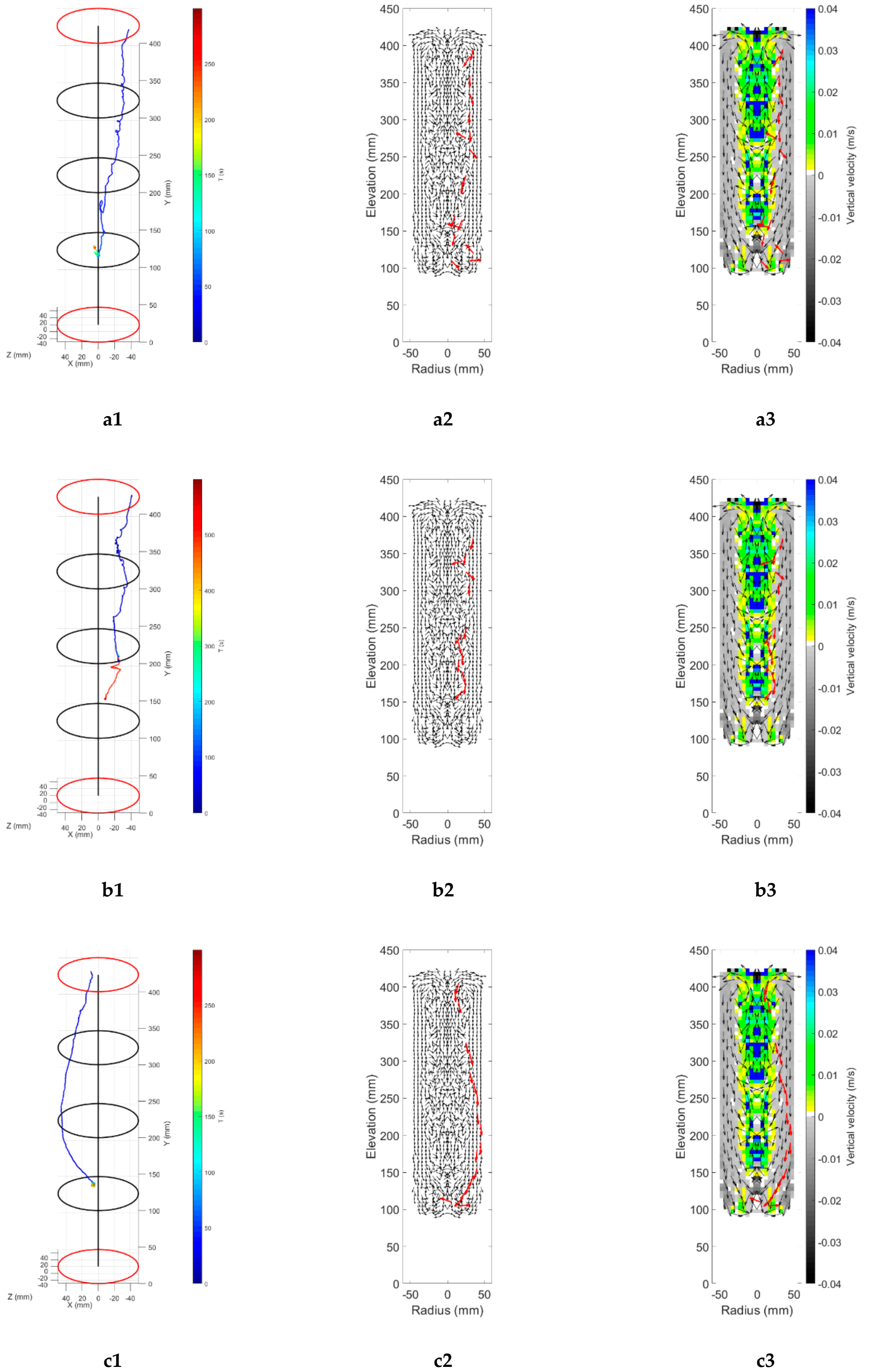

Figure 3. The results of 3 runs (**a**–**c**) of −300 + 212 μm hematite particle for an airflow rate of 1.25 u_{mf} (Lagrangian trajectory (1) and Eulerian flow maps (2 and 3)).

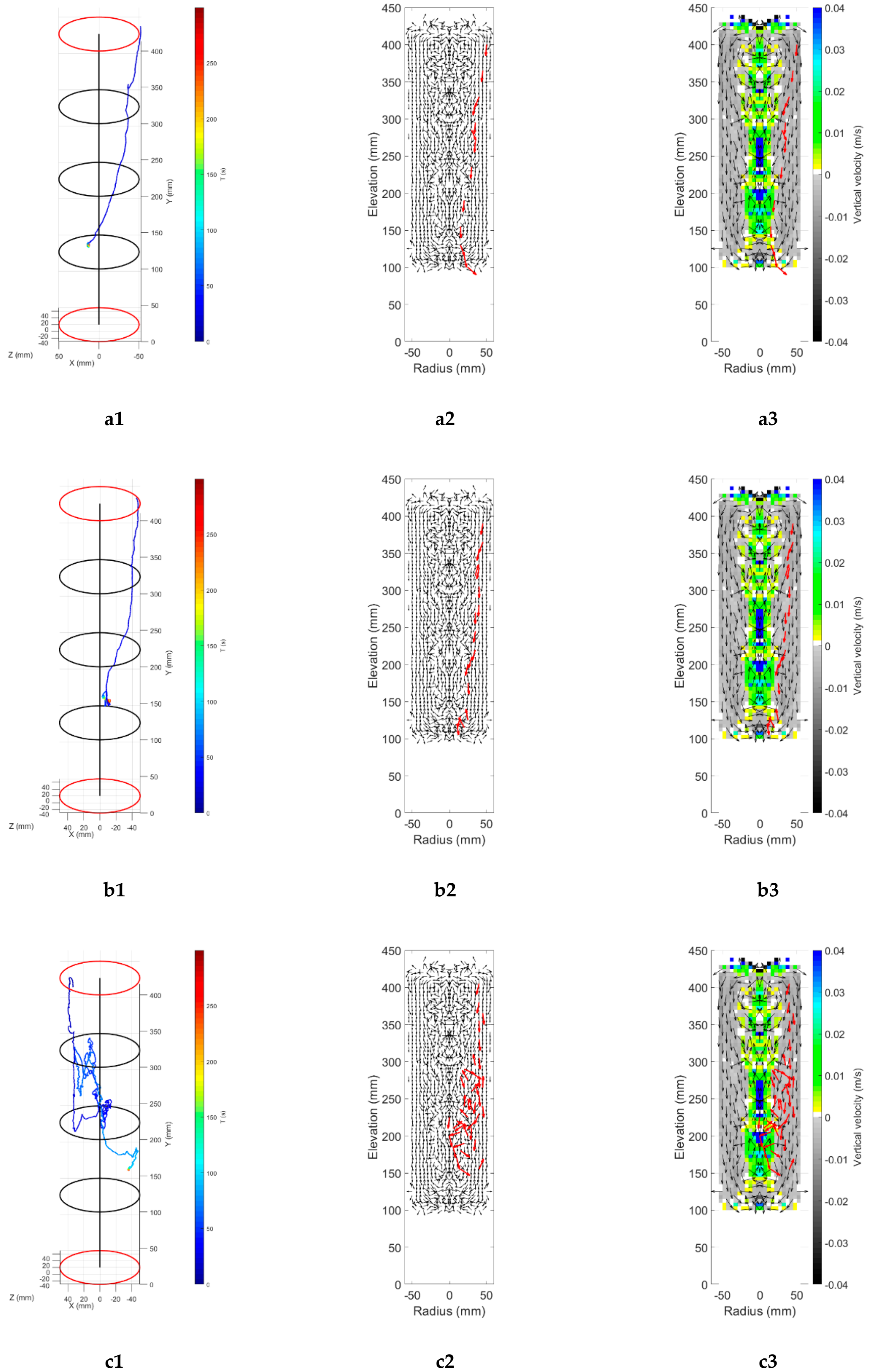

Figure 4. The results of 3 runs (**a**–**c**) of −300 + 212 µm hematite particle for an airflow rate of 1.50 u_{mf} (Lagrangian trajectory (1) and Eulerian flow maps (2 and 3)).

3.2.2. The −212 + 150 µm Hematite Bed

Figures 5 and 6 show the results of the two runs (a and b) for the −212 + 150 µm hematite particle with an airflow rate of 1.25 u_{mf} and 1.50 u_{mf}, respectively.

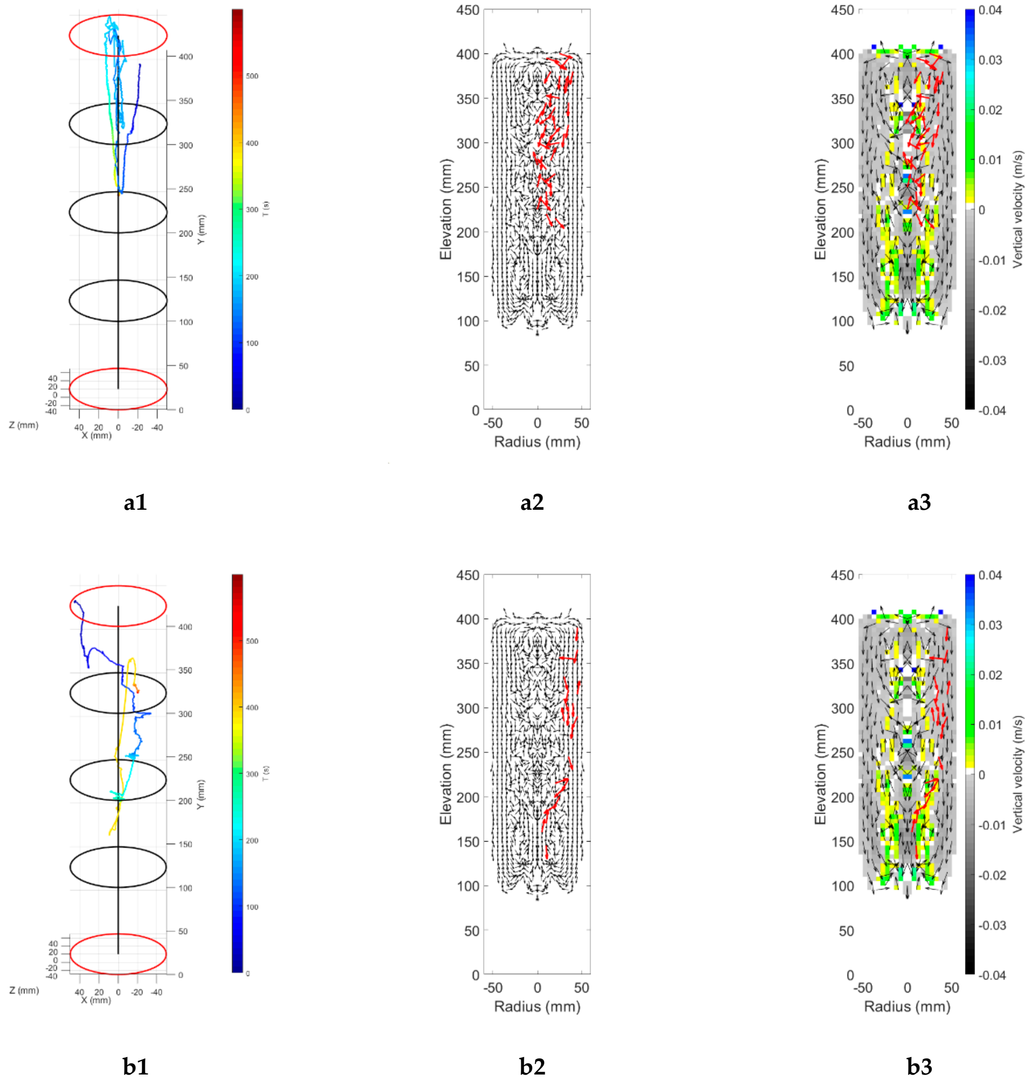

Figure 5. The results of 2 runs (**a**,**b**) of a −212 + 150 μm hematite particle for an airflow rate of 1.25 u_{mf} (Lagrangian trajectory (1) and Eulerian flow maps (2 and 3)).

It was observed that, even though the tracer did not stay at the bottom, some hematite particles fed to the fluidized bed reached the bottom and remained there. However, even though there was a separation, the recovery of the heavy particles would be lower than coarse bed (−300 + 212 μm) separation. Regardless of the low recovery, it shows that there is still a potential for separation in this size fraction.

For further investigation, experiments at the 1.50 u_{mf} airflow rate were conducted. However, the particle did not descend. On the contrary, it started to travel all over the bed with the bulk quartz material (Figure 6(a1,a2)). The observation of the bulk hematite particles showed a similar trend as the tracer particle. They were distributed in the bed, nearly homogeneously, and acted like the bed material.

Based on Eulerian flow maps of this size fraction (Figure 6(a2,a3,b2,b3)), the descending velocity of the dense particle was similar to that of the bulk bed particle, while the ascending velocity of the heavy particle was slightly slower than the bed particle. This indicates that, during the ascension, the gravity forces are still effective. However, they are not sufficient to overcome the effect of the airflow. From these results, it can be concluded that, for this size fraction, lower airflow rates (<1.25 u_{mf}) should be investigated to produce a better separation.

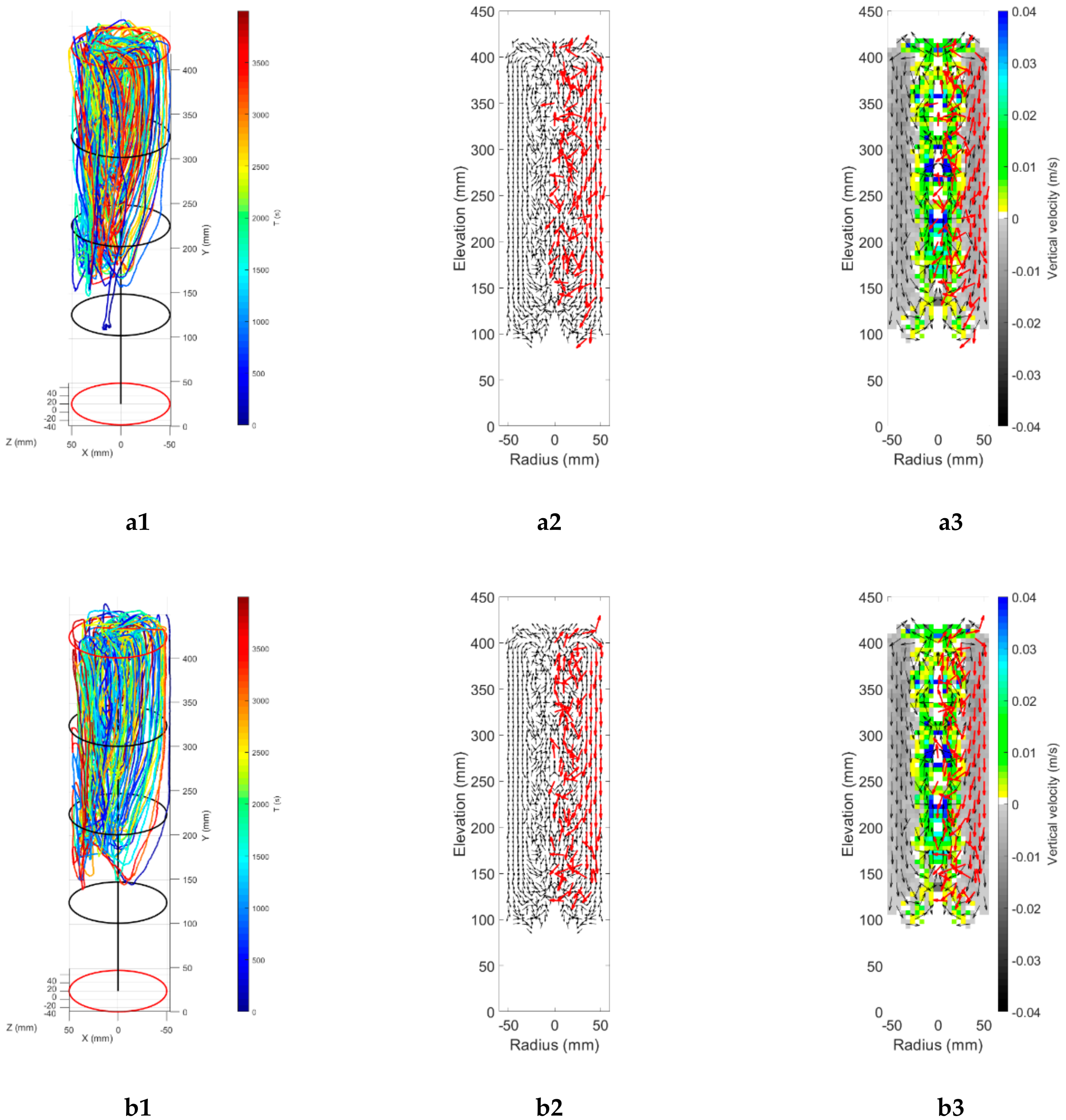

Figure 6. The results of 2 runs (**a**,**b**) of a −212 + 150 µm hematite particle for an airflow rate of 1.50 u_{mf} (Lagrangian trajectory (1) and Eulerian flow maps (2 and 3)).

Even though there was no observable separation, the results indicate that mixing the light (quartz) and heavy (hematite) material in this size fraction can be useful for creating denser beds.

3.2.3. The −150 + 106 µm Hematite Bed

Figures 7 and 8 show the results of the two runs (a and b) for the −150 + 106 µm hematite particle with an airflow rate of 1.25 u_{mf} and 1.50 u_{mf}, respectively.

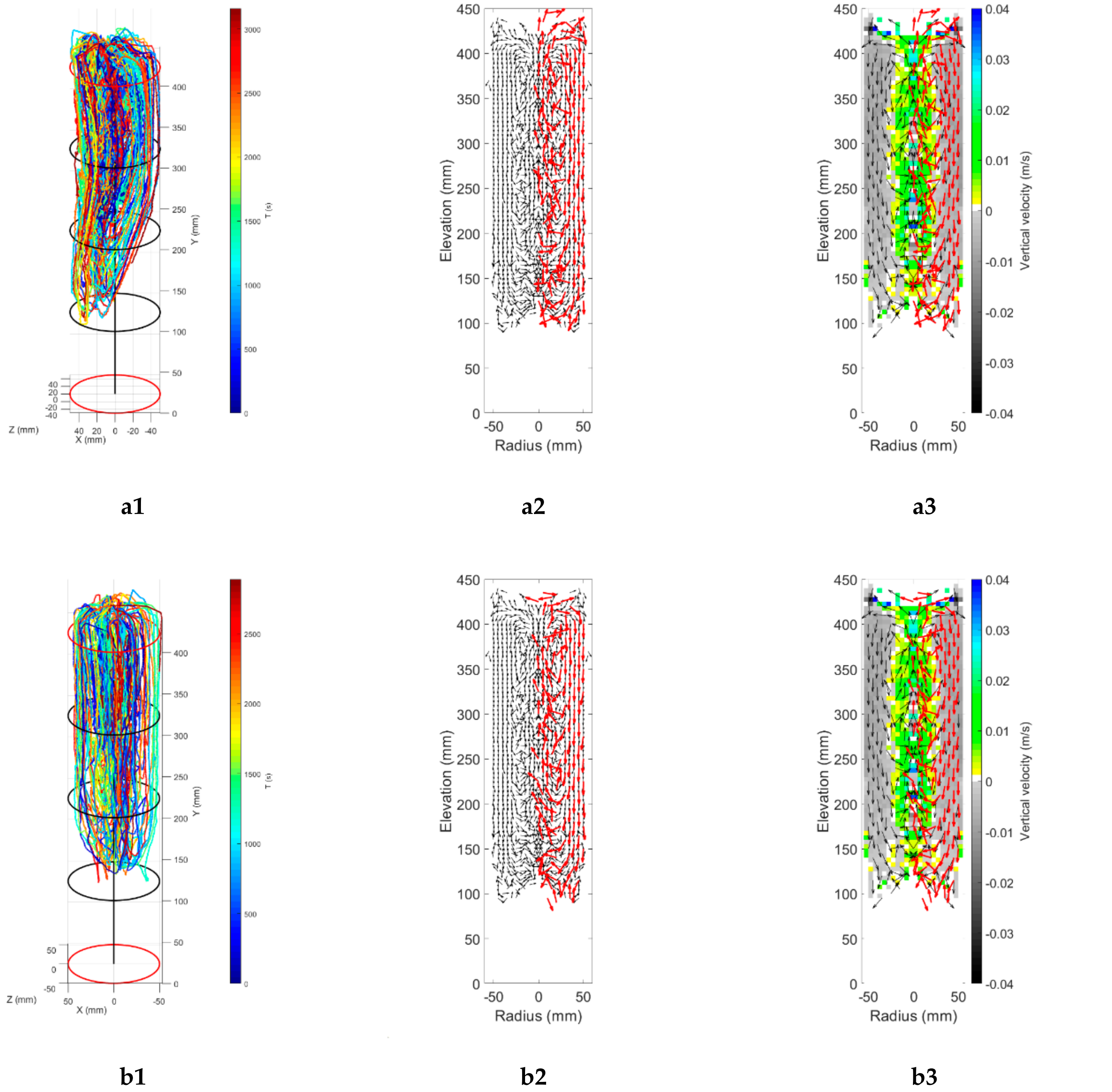

Figure 7. The results of 2 runs (**a**,**b**) of the −150 + 106 μm hematite particle for an airflow rate of 1.25 u_{mf} (Lagrangian trajectory (1) and Eulerian flow maps (2 and 3)).

As can be seen from the particle trajectories (Figure 7(a1,b1) and Figure 8(a1,b1)), the heavy particles acted like a bed particle and did not remain at the bottom of the bed during the two runs regardless of the airflow rate. In each case, the particle descended in the descending bed region, and then started to rise with the airflow following the same route and with the same velocity as the bed particles (Figure 7(a2,a3,b2,b3) and Figure 8(a2,a3,b2,b3)). This shows that both heavy and light particles travel all over the cylinder at the same trajectory. The reason for this is that the high absolute velocity of the ascending region pushing the particle upward in the center overcomes the downward impact of gravity on the heavy particle. It can be concluded that there will likely be no separation in a deep bed created from particles of this size. However, it is possible to make a homogeneous high-density bed which can be potentially used as bed material for dry dense medium separation of iron ore based on floating and sinking of ore particles in a gas–solid fluidized bed. Based on the good mixing behavior, this bed also has the potential to be applied to tribocharging mineral particles prior to using a triboelectric separator.

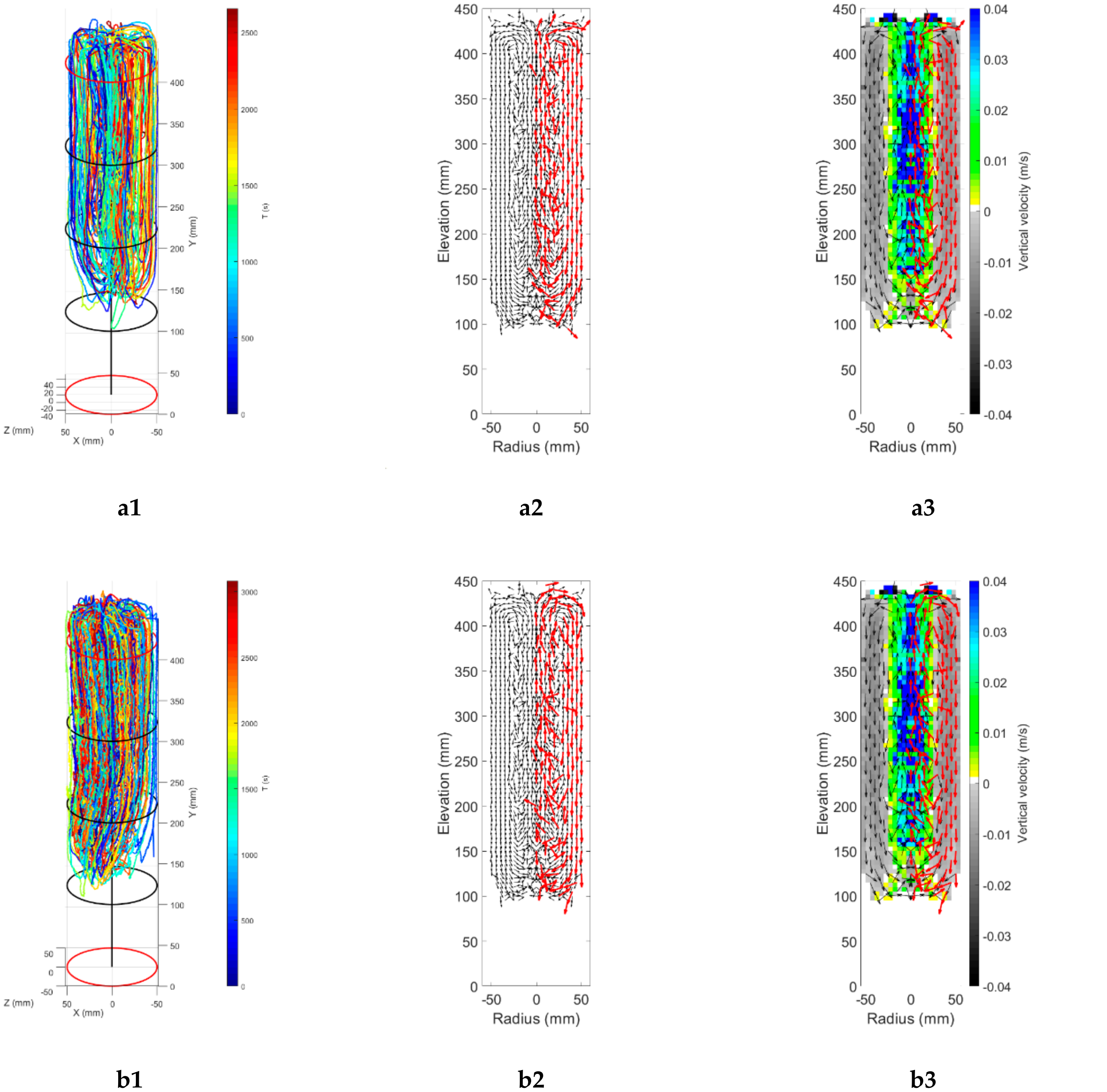

Figure 8. The results of 2 runs (**a**,**b**) of the −150 + 106 µm hematite particle for an airflow rate of 1.50 u_{mf} (Lagrangian trajectory (1) and Eulerian flow maps (2 and 3)).

3.3. General Discussion

Symmetric circulating particle flow formed where the particles rose along the center area of the bed and move to the wall sides after reaching the top, and descended along the wall. This observed fluidized bed motion behavior from the PEPT tests is similar to that reported previously by Luo et al. [71], in which CFD–DEM simulation was applied for modeling. The circulating particle flow became strong as the superficial air velocity increased, which corresponds well with the findings from Oshitani et al. [117].

Regarding the separation behavior, the coarsest size (−300 + 212 µm) achieved best separation regardless of the airflow rates. Density segregation dominates the separation since the heavy hematite and light quartz are controlled in the same size fraction for each test to minimize the effect of size segregation. Hematite settles faster than quartz under the flow and separation happens as the drag force from the ascending airflow cannot compete with the gravity force acting on particles in the coarse size fraction. It should be noted that, even in the coarsest size fraction, there is a chance for heavy particles to be entrained (third run of the −300 + 212 μm fraction under high airflow rate). However, the particles of this size eventually overcame the hindered effect from the rising flow and managed to percolate through the fluidized bed to reach the bottom of the bed to form the final concentrate. This finding may indicate that high airflow could result in a longer separation time for coarse sizes. Overall, the degree of the density segregation depends on the air velocity. The segregation dependence on the air velocity is related to the difference in the size of the air bubbles and the fluidization intensity in various locations of the bed. Oshitani et al. [26] came to the same conclusion when they treated iron ore in similar size range in a gas–solid fluidized bed.

The negative effect of increasing airflow rate on separation performance becomes more pronounced in finer size fractions, since the drag force dominated the flow motion of particles. There was no observed separation, and hematite and quartz particles mixed well and travelled all over the bed. There was no difference when compared to the solid mixing model presented in the literature [71]. The overall behavior of the tracer particle is representative of the bulk motion as the single particle had been followed for a long-enough period (one hour) [118]. As the airflow rate increases, particulate collisions happen more frequently, which corresponds well with the observations from Lagrangian trajectory figures. This can develop more convective cells in the bed at different heights. Finer heavy particles become entrained easily. It is possible that particles still separate briefly on the micro-scale at an individual trajectory level, then become entrained easily in these local convection cells and/or become re-entrained in another cell after a longer period. Thus, the motion behavior looks similar on average over time and no separation is observed overall.

4. Conclusions

This paper presents the characterization of mono-sized (−300 + 212, −212 + 150, −150 + 106 μm) deep beds and an investigation into the separation mechanism of heavy particles in a fluidized bed using PEPT. The conclusions are as follows:

1. Quartz (a typical Geldart Group B solid) and hematite can be activated for PEPT characterization of the fluidized bed and investigations into the separation mechanisms.
2. The overall bulk motion is nearly the same, which indicates that the average bed behavior is very systematic and as described in the literature. Despite their different ascending and descending velocities, bed material of all sizes show the same patterns as described by Kunii and Levenspiel [41] and Lin et al. [80].
3. The coarsest size fraction (−300 + 212 μm) yields the best separation. The heavy hematite particle descends in less than 5 min under both airflow rates. However, increasing the airflow rate increases the chance of the heavy particle being entrained by the increasing ascending flow, which results in longer separation time.
4. Separation happens in the −212 + 150 μm fraction with a lower airflow rate (1.25 u_{mf}); the recovery will, however, be low due to the hindering effect from the bulk ascending flow. There is no separation under a higher airflow rate.
5. There is no observed separation at −150 + 106 μm fraction. However, the similar flow patterns of the light and dense particles in this case can possibly be used for creating high-density beds.

Fine-size separation can be possible in a dry fluidized bed; however, more work should be conducted focusing on different fluidized bed heights and/or a different size and shape of the bed structure.

Author Contributions: Conceptualization, M.Z., O.K. and K.E.W.; methodology, M.Z., O.K. and T.W.L.; software, T.W.L., D.B. and M.L.; validation, M.Z. and O.K.; formal analysis, M.Z. and O.K.; investigation, M.Z., O.K. and R.L.; resources, T.W.L. and K.E.W.; data curation, M.Z., O.K. and T.W.L.; writing—original draft preparation, M.Z. and O.K.; writing—review and editing, O.K., M.Z. and K.E.W.; visualization, M.Z., O.K. and K.E.W.; supervision, K.E.W.; project administration, K.E.W.; funding acquisition, K.E.W. All authors have read and agreed to the published version of the manuscript.

Funding: This research was funded by the Natural Science and Engineering Research Council of Canada (NSERC) in conjunction with SGS Canada Inc., COREM, Teck Resources Ltd., and Flottec, through the Collaborative Research and Development Grant Program (CRDPJ-531957-18). M. Zhou and M. Lepage would also like to acknowledge funding from the McGill Engineering Doctoral Award.

Data Availability Statement: The data presented in this study are available on request from the corresponding author. The data are not publicly available due to privacy.

Conflicts of Interest: The authors declare no conflict of interest.

Appendix A

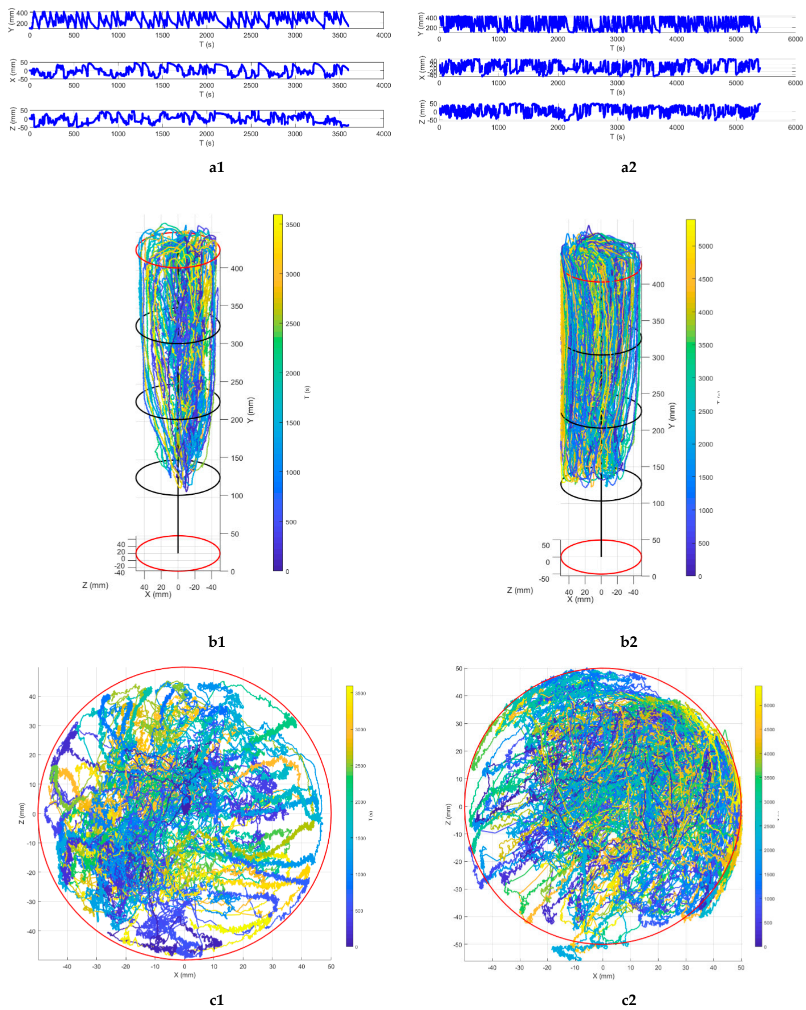

Figure A1. Trajectories of an activated quartz particle (−300 + 212 μm) inside the bed against time for 1.25 u_{mf} (1) and 1.50 u_{mf} (2): (**a**) the tracer trajectory with fit; the tracer trajectory from side view (**b**) and top view (**c**).

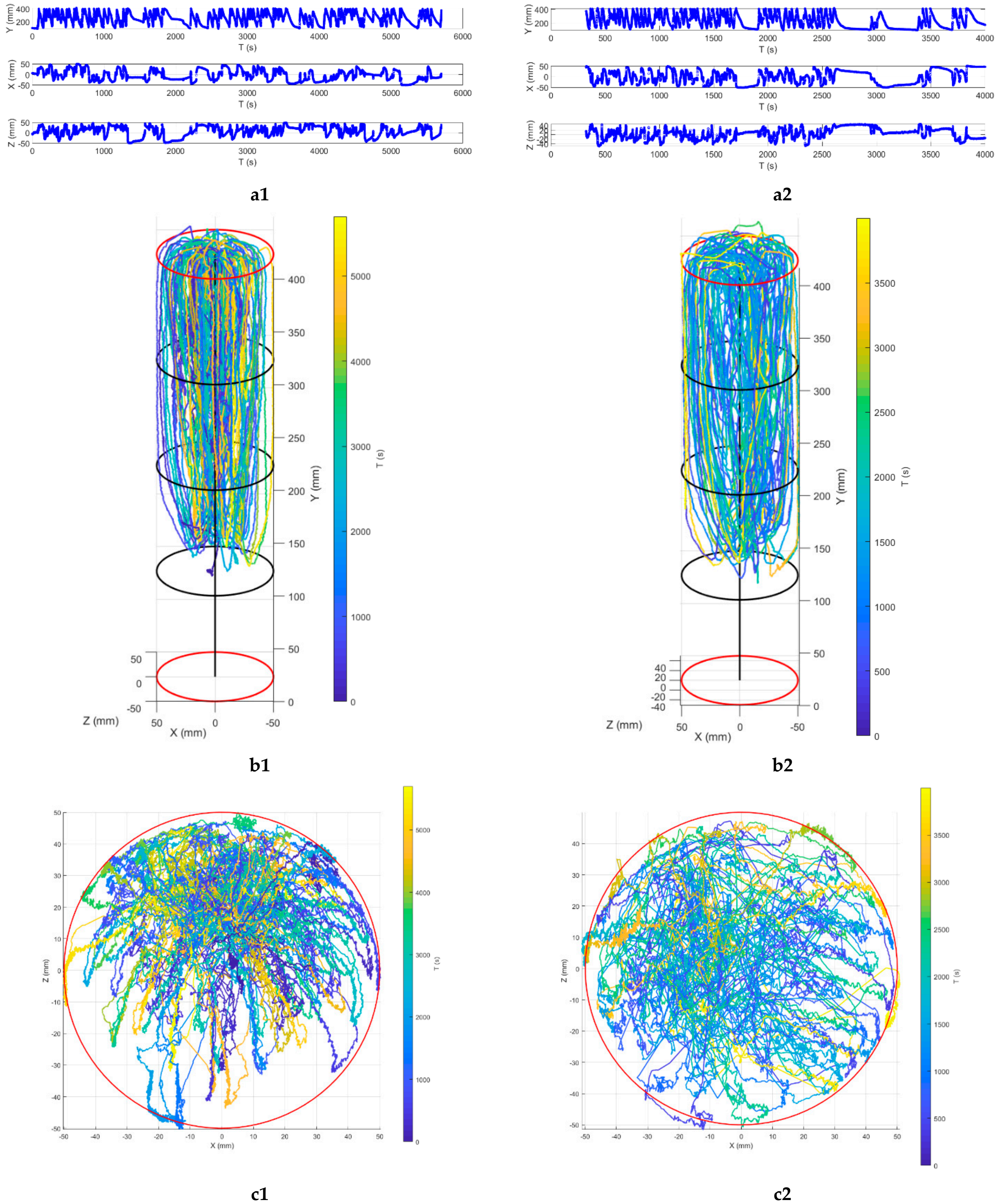

Figure A2. Trajectories of an activated quartz particle (−212 + 150 μm) inside the bed against time for 1.25 u_{mf} (1) and 1.50 u_{mf} (2): (**a**) the tracer trajectory with fit; the tracer trajectory from side view (**b**) and top view (**c**).

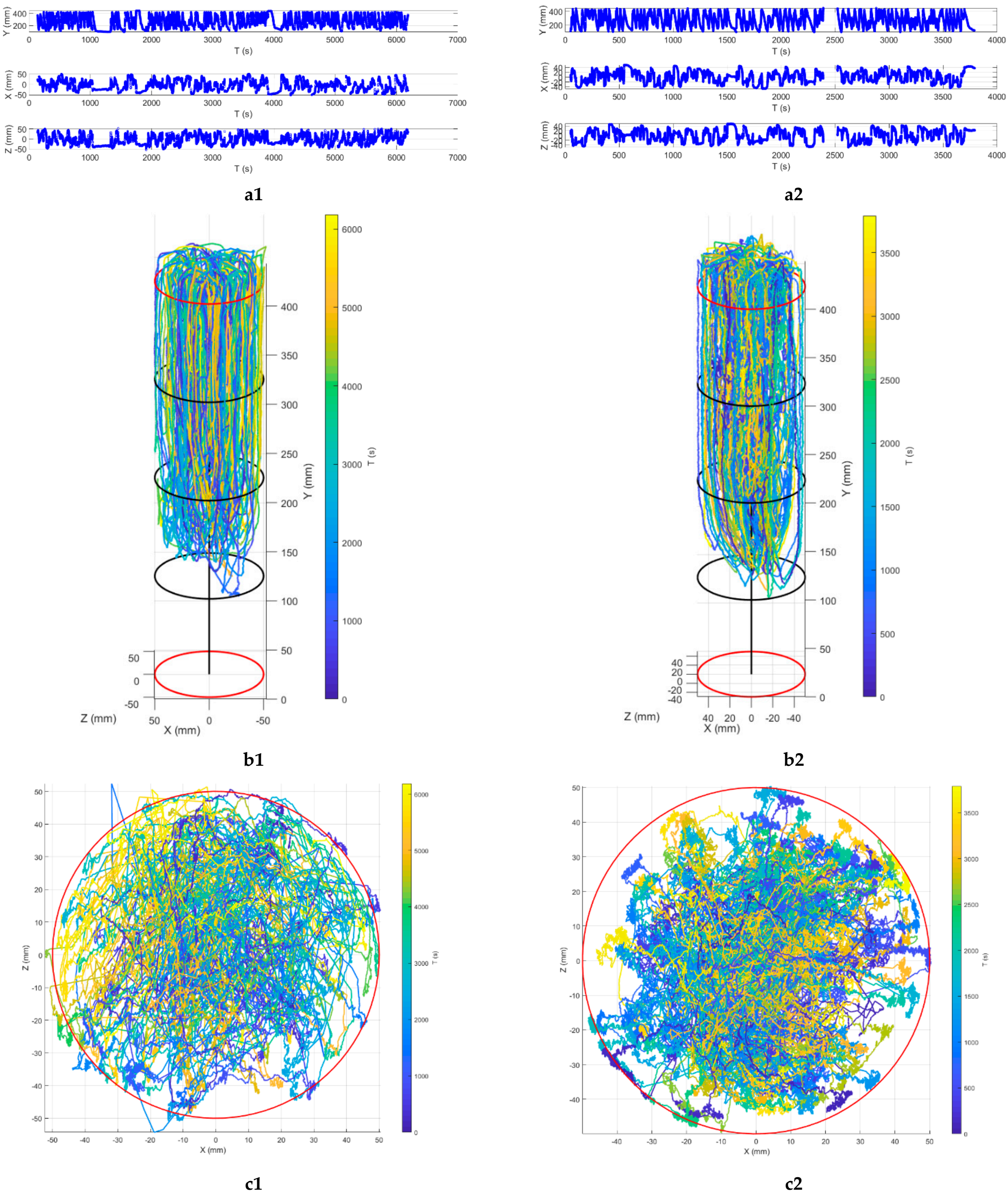

Figure A3. Trajectories of an activated quartz particle (−150 + 106 μm) inside the bed against time for 1.25 u_{mf} (1) and 1.50 u_{mf} (2): (**a**) the tracer trajectory with fit; the tracer trajectory from side view (**b**) and top view (**c**).

References

1. WWAP. *WWAP (United Nations World Water Assessment Programme). 2017. The United Nations World Water Development Report 2017: Wastewater, The Untapped Resource*; UNESCO: Paris, France, 2017.
2. Fekete, B.M. 5.02—State of the World's Water Resources. In *Reference Module in Earth Systems and Environmental Sciences, Climate Vulnerability*; Volume 5: Vulnerability of Water Resources to Climate; Academic Press: Oxford, UK, 2013; pp. 11–23.
3. Boretti, A.; Rosa, L. Reassessing the projections of the World Water Development Report. *NPJ Clean Water* **2019**, *2*, 15. [CrossRef]
4. UNESCO on behalf of UN-Water. *United Nations World Water Development Report 2020: Water and Climate Change*; UNESCO: Paris, France, 2020; Available online: https://unesdoc.unesco.org/ark:/48223/pf0000372985.locale=en (accessed on 6 January 2021).
5. Leveque, B.; Burnet, J.B.; Dorner, S.; Bichai, F. Impact of climate change on the vulnerability of drinking water intakes in a northern region. *Sustain. Cities Soc.* **2021**, *66*, 102656. [CrossRef]
6. Debaere, P.; Kapral, A. The potential of the private sector in combating water scarcity: The economics. *Water Secur.* **2021**, *13*, 100090. [CrossRef]
7. Katyaini, S.; Barua, A.; Duarte, R. Science-policy interface on water scarcity in India: Giving 'visibility' to unsustainable virtual water flows (1996–2014). *J. Clean. Prod.* **2020**, *275*, 124059. [CrossRef]
8. Habiyaremye, A. Water innovation in South Africa: Mapping innovation successes and diffusion constraints. *Environ. Sci. Policy* **2020**, *114*, 217–229. [CrossRef]
9. Alvez, A.; Aitken, D.; Rivera, D.; Vergara, M.; McIntyre, N.; Concha, F. At the crossroads: Can desalination be a suitable public policy solution to address water scarcity in Chile's mining zones? *J. Environ. Manage.* **2020**, *258*, 110039. [CrossRef] [PubMed]
10. Jiang, Y. China's water scarcity. *J. Environ. Manage.* **2009**, *90*, 3185–3196. [CrossRef]
11. He, J.; Zhao, Y.; He, Y.; Luo, Z.; Li, H.; Duan, C. Hydrodynamic characteristics of the dense medium gas–solid fluidized bed for coal beneficiation and cleaning. *Part. Sci. Technol.* **2016**, *34*, 173–183. [CrossRef]
12. He, J.; Tan, M.; Zhao, Y.; Duan, C.; He, Y.; Luo, Z. Fluidization characteristics and density-based separation of dense-medium gas–solid fluidized bed: An experimental and simulation study. *J. Taiwan Inst. Chem. Eng.* **2016**, *61*, 223–233. [CrossRef]
13. Zhao, Y.; Yang, X.; Luo, Z.; Duan, C.; Song, S. Progress in developments of dry coal beneficiation. *Int. J. Coal. Sci. Technol.* **2014**, *1*, 103–112. [CrossRef]
14. Yang, X.; Zhao, Y.; Luo, Z.; Song, S.; Chen, Z. Fine coal dry beneficiation using autogenous medium in a vibrated fluidized bed. *Int. J. Miner. Process.* **2013**, *125*, 86–91. [CrossRef]
15. Wang, Q.; Lu, J.; Yin, W.; Yang, H.; Wei, L. Numerical study of gas–solid flow in a coal beneficiation fluidized bed using kinetic theory of granular flow. *Fuel Process. Technol.* **2013**, *111*, 29–41. [CrossRef]
16. Firdaus, M.; O'Shea, J.-P.; Oshitani, J.; Franks, G.V. Beneficiation of Coarse Coal Ore in an Air-Fluidized Bed Dry Dense-Medium Separator. *Int. J. Coal Prep. Util.* **2012**, *32*, 276–289. [CrossRef]
17. Macpherson, S.A.; Iveson, S.M.; Galvin, K.P. Density-based separation in a vibrated Reflux Classifier with an air-sand dense-medium: Tracer studies with simultaneous underflow and overflow removal. *Miner. Eng.* **2011**, *24*, 1046–1052. [CrossRef]
18. Macpherson, S.A.; Iveson, S.M.; Galvin, K.P. Density based separations in the Reflux Classifier with an air–sand dense–medium and vibration. *Miner. Eng.* **2010**, *23*, 74–82. [CrossRef]
19. Macpherson, S.A.; Galvin, K.P. The Effect of Vibration on Dry Coal Beneficiation in the Reflux Classifier. *Int. J. Coal Prep. Util.* **2010**, *30*, 283–294. [CrossRef]
20. Sahu, A.K.; Biswal, S.K.; Parida, A. Development of Air Dense Medium Fluidized Bed Technology For Dry Beneficiation of Coal—A Review. *Int. J. Coal Prep. Util.* **2009**, *29*, 216–241. [CrossRef]
21. Dwari, R.K.; Rao, K.H. Dry Beneficiation of Coal—A Review. *Miner. Process. Extr. Metall. Rev.* **2007**, *28*, 177–234. [CrossRef]
22. Oshitani, J.; Franks, G.V.; Griffin, M. Dry dense medium separation of iron ore using a gas–solid fluidized bed. *Adv. Powder Technol.* **2010**, *21*, 573–577. [CrossRef]
23. Oshitani, J.; Isei, Y.; Yoshida, M.; Gotoh, K.; Franks, G.V. Influence of air bubble size on float–sink of spheres in a gas–solid fluidized bed. *Adv. Powder Technol.* **2012**, *23*, 120–123. [CrossRef]
24. Oshitani, J.; Kajimoto, S.; Yoshida, M.; Franks, G.V.; Kubo, Y.; Nakatsukasa, S. Continuous float–sink density separation of lump iron ore using a dry sand fluidized bed dense medium. *Adv. Powder Technol.* **2013**, *24*, 468–472. [CrossRef]
25. Oshitani, J.; Kawahito, T.; Yoshida, M.; Gotoh, K.; Franks, G.V. The influence of the density of a gas–solid fluidized bed on the dry dense medium separation of lump iron ore. *Miner. Eng.* **2011**, *24*, 70–76. [CrossRef]
26. Oshitani, J.; Ohnishi, M.; Yoshida, M.; Franks, G.V.; Kubo, Y.; Nakatsukasa, S. Dry separation of particulate iron ore using density-segregation in a gas–solid fluidized bed. *Adv. Powder Technol.* **2013**, *24*, 554–559. [CrossRef]
27. Franks, G.V.; Firdaus, M.; Oshitani, J. Copper ore density separations by float/sink in a dry sand fluidised bed dense medium. *Int. J. Miner. Process.* **2013**, *121*, 12–20. [CrossRef]
28. Franks, G.V.; Forbes, E.; Oshitani, J.; Batterham, R.J. Economic, water and energy evaluation of early rejection of gangue from copper ores using a dry sand fluidised bed separator. *Int. J. Miner. Process.* **2015**, *137*, 43–51. [CrossRef]
29. Kökkılıç, O.; Langlois, R.; Waters, K.E. A design of experiments investigation into dry separation using a Knelson Concentrator. *Miner. Eng.* **2015**, *72*, 73–86. [CrossRef]
30. Zhou, M.; Kökkılıç, O.; Langlois, R.; Waters, K.E. Size-by-size analysis of dry gravity separation using a 3-in. *Knelson Concentrator. Miner. Eng.* **2016**, *91*, 42–54. [CrossRef]

31. Beeckmans, J.M. *Dry Separation of Plastics by Density Using Fluidized Bed Technology*; Waste Management Branch, Ontario Ministry of the Environment: Ottawa, ON, Canada, 1992.
32. Oshitani, J.; Kajiwara, T.; Kiyoshima, K.; Tanaka, Z. Separation of Automobile Shredder Residue by Gravity Separation Using a Gas-Solid Fluidized Bed [Translated]. *Kona Powder Part. J.* **2003**, *21*, 185–194. [CrossRef]
33. Sekito, T.; Matsuto, T.; Tanaka, N. Application of a gas–solid fluidized bed separator for shredded municipal bulky solid waste separation. *Waste Manag.* **2006**, *26*, 1422–1429. [CrossRef]
34. Sekito, T.; Tanaka, N.; Matsuto, T. Batch separation of shredded bulky waste by gas–solid fluidized bed at laboratory scale. *Waste Manag.* **2006**, *26*, 1246–1252. [CrossRef] [PubMed]
35. Yoshida, M.; Nakatsukasa, S.; Nanba, M.; Gotoh, K.; Zushi, T.; Kubo, Y.; Oshitani, J. Decrease of Cl contents in waste plastics using a gas–solid fluidized bed separator. *Adv. Powder Technol.* **2010**, *21*, 69–74. [CrossRef]
36. Han, Y.; He, W.; Li, L.; Li, G.; Huang, J. Mathematical analysis of the gas–solid fluidized bed separation of metals and nonmetals from waste PCB powders. *Powder Technol.* **2016**, *295*, 142–151. [CrossRef]
37. Chehreh Chelgani, S.; Nasiri, H.; Tohry, A. Modeling of particle sizes for industrial HPGR products by a unique explainable AI tool- A "Conscious Lab" development. *Adv. Powder Technol.* **2021**, *32*, 4141–4148. [CrossRef]
38. Li, G.; Roufail, R.; Klein, B.; Nordell, L.; Kumar, A.; Sun, C.; Kou, J. Experimental evaluation of the conjugate anvil hammer mill—Comparison of semi-confined to confined particle breakage. *Miner. Eng.* **2019**, *137*, 34–42. [CrossRef]
39. Nordell, L.; Potapov, A. Novel Comminution Machine May Vastly Improve Crushing-Grinding Efficiency. In Proceedings of the 6th International Conference on Semi-Autogenous and High Pressure Grinding Technology (SAG 15), Vancouver, BC, Canada, 20–24 September 2015.
40. Nordell, L.K.; Porter, B.; Potapor, A. Comminution Energy Efficiency—Understanding the Next Steps. In Proceedings of the XXVIII Int. Mineral Processing Congress, Quebec City, QC, Canada, 11–15 September 2016.
41. Kunii, D.; Levenspiel, O. *Fluidization Engineering*, 2nd ed.; Butterworth-Heinemann: Waltham, MA, USA, 1991.
42. Perry, R.H.; Green, D.W.; Maloney, J.O. *Perry's Chemical Engineers' Handbook*, 7th ed.; McGraw-Hill Professional Publishing: New York, USA, 1997.
43. Yang, W.C. *Handbook of Fluidization and Fluid-Particle Systems*; CRC Press: Boca Raton, FL, USA, 2003.
44. Oka, S. *Fluidized Bed Combustion*; CRC Press: Boca Raton, FL, USA, 2003.
45. Guan, Y.; Chang, J.; Zhang, K.; Wang, B.; Sun, Q. Three-dimensional CFD simulation of hydrodynamics in an interconnected fluidized bed for chemical looping combustion. *Powder Technol.* **2014**, *268*, 316–328. [CrossRef]
46. Raganati, F.; Ammendola, P.; Chirone, R. Effect of acoustic field on CO2 desorption in a fluidized bed of fine activated carbon. *Particuology* **2015**, *23*, 8–15. [CrossRef]
47. Weber, J.M.; Stehle, R.C.; Breault, R.W.; De Wilde, J. Experimental study of the application of rotating fluidized beds to particle separation. *Powder Technol.* **2017**, *316*, 123–130. [CrossRef]
48. Tahmasebi, A.; Yu, J.; Han, Y.; Zhao, H.; Bhattacharya, S. A kinetic study of microwave and fluidized-bed drying of a Chinese lignite. *Chem. Eng. Res. Des.* **2014**, *92*, 54–65. [CrossRef]
49. Meyer, K.; Bück, A.; Tsotsas, E. Determination of particle exchange rates at over-flow weirs in horizontal fluidised beds by particle tracking velocimetry. *Particuology* **2017**, *32*, 1–9. [CrossRef]
50. Promvonge, P.; Boonloi, A.; Pimsarn, M.; Thianpong, C. Drying characteristics of peppercorns in a rectangular fluidized-bed with triangular wavy walls. *Int. Commun. Heat Mass Transf.* **2011**, *38*, 1239–1246. [CrossRef]
51. Boissiere, B.; Ansart, R.; Gauthier, D.; Flamant, G.; Hemati, M. Experimental hydrodynamic study of gas-particle dense suspension upward flow for application as new heat transfer and storage fluid. *Can. J. Chem. Eng.* **2015**, *93*, 317–330. [CrossRef]
52. Depypere, F.; Pieters, J.G.; Dewettinck, K. PEPT visualisation of particle motion in a tapered fluidised bed coater. *J. Food Eng.* **2009**, *93*, 324–336. [CrossRef]
53. Lan, R.; Liu, Y.; Wang, G.; Wang, T.; Kan, C.; Jin, Y. Experimental modeling of polymer latex spray coating for producing controlled-release urea. *Particuology* **2011**, *9*, 510–516. [CrossRef]
54. Gorji-Kandi, S.; Alavi-Amleshi, S.M.; Mostoufi, N. A solids mixing rate correlation for small scale fluidized beds. *Particuology* **2015**, *21*, 55–64. [CrossRef]
55. Xie, H.; Sun, Z. Mass transfer between bubbles and the dense phase in gas fluidized beds. *Particuology* **2014**, *16*, 213–217. [CrossRef]
56. Krüger, B.; Mrotzek, A.; Wirtz, S. Separation of harmful impurities from refuse derived fuels (RDF) by a fluidized bed. *Waste Manage.* **2014**, *34*, 390–401. [CrossRef]
57. Rhodes, M. *Introduction to Particle Technology*, 2nd ed.; Wiley: Chichester, UK, 2008.
58. Ireland, E.; Pitt, K.; Smith, R. A review of pulsed flow fluidisation; the effects of intermittent gas flow on fluidised gas–solid bed behaviour. *Powder Technol.* **2016**, *292*, 108–121. [CrossRef]
59. Oshitani, J.; Kondo, M.; Nishi, H.; Tanaka, Z. Separation of silicastone and pyrophyllite by a gas-solid fluidized bed utilizing slight difference of density. *Adv. Powder Technol.* **2003**, *14*, 247–258. [CrossRef]
60. Zhao, P.; Zhao, Y.; Chen, Z.; Luo, Z. Dry cleaning of fine lignite in a vibrated gas-fluidized bed: Segregation characteristics. *Fuel* **2015**, *142*, 274–282. [CrossRef]
61. Oshitani, J.; Teramoto, K.; Yoshida, M.; Kubo, Y.; Nakatsukasa, S.; Franks, G.V. Dry beneficiation of fine coal using density-segregation in a gas–solid fluidized bed. *Adv. Powder Technol.* **2016**, *27*, 1689–1693. [CrossRef]

62. Tebianian, S.; Dubrawski, K.; Ellis, N.; Cocco, R.A.; Hays, R.; Reddy Karri, S.B.; Leadbeater, T.W.; Parker, D.J.; Chaouki, J.; Jafari, R.; et al. Investigation of particle velocity in FCC gas-fluidized beds based on different measurement techniques. *Chem. Eng. Sci.* **2015**, *127*, 310–322. [CrossRef]
63. Horio, M.; Kuroki, H. Three-dimensional flow visualization of dilutely dispersed solids in bubbling and circulating fluidized beds. *Chem. Eng. Sci.* **1994**, *49*, 2413–2421. [CrossRef]
64. Rhodes, M.; Mineo, H.; Hirama, T. Particle motion at the wall of a circulating fluidized bed. *Powder Technol.* **1992**, *70*, 207–214. [CrossRef]
65. Hagemeier, T.; Roloff, C.; Bück, A.; Tsotsas, E. Estimation of particle dynamics in 2-D fluidized beds using particle tracking velocimetry. *Particuology* **2015**, *22*, 39–51. [CrossRef]
66. Roy, S.; Pant, H.J.; Roy, S. Velocity characterization of solids in binary fluidized beds. *Chem. Eng. Sci.* **2021**, *246*, 116883. [CrossRef]
67. Wang, Q.; Niemi, T.; Peltola, J.; Kallio, S.; Yang, H.; Lu, J.; Wei, L. Particle size distribution in CPFD modeling of gas–solid flows in a CFB riser. *Particuology* **2015**, *21*, 107–117. [CrossRef]
68. Chladek, J.; Jayarathna, C.K.; Moldestad, B.M.E.; Tokheim, L.-A. Fluidized bed classification of particles of different size and density. *Chem. Eng. Sci.* **2018**, *177*, 151–162. [CrossRef]
69. Alobaid, F.; Baraki, N.; Epple, B. Investigation into improving the efficiency and accuracy of CFD/DEM simulations. *Particuology* **2014**, *16*, 41–53. [CrossRef]
70. Han, Q.; Yang, N.; Zhu, J.; Liu, M. Onset velocity of circulating fluidization and particle residence time distribution: A CFD–DEM study. *Particuology* **2015**, *21*, 187–195. [CrossRef]
71. Luo, K.; Wu, F.; Yang, S.; Fan, J. CFD–DEM study of mixing and dispersion behaviors of solid phase in a bubbling fluidized bed. *Powder Technol.* **2015**, *274*, 482–493. [CrossRef]
72. Zhao, Y.; Tang, L.; Luo, Z.; Liang, C.; Xing, H.; Wu, W.; Duan, C. Experimental and numerical simulation studies of the fluidization characteristics of a separating gas–solid fluidized bed. *Fuel Process. Technol.* **2010**, *91*, 1819–1825. [CrossRef]
73. He, J.; Tan, M.; Zhu, R.; Zhao, Y.; Luo, Z.; Duan, C. Process optimization for coal cleaning by enhancing the air-distribution stability of dry separator. *Powder Technol.* **2016**, *288*, 45–54. [CrossRef]
74. Kumar, D.; Iveson, S.M.; Galvin, K.P. Dry separation using a fluidized Sink-Hole. *Miner. Eng.* **2018**, *127*, 105–113. [CrossRef]
75. Hawkesworth, M.R.; O'Dwyer, M.A.; Walker, J.; Fowles, P.; Heritage, J.; Stewart, P.A.E.; Witcomb, R.C.; Bateman, J.E.; Connolly, J.F.; Stephenson, R. A positron camera for industrial application. *Nucl. Instrum. Methods Phys. Res. Sect. A* **1986**, *253*, 145–157. [CrossRef]
76. Parker, D.J.; Broadbent, C.J.; Fowles, P.; Hawkesworth, M.R.; McNeil, P. Positron emission particle tracking—A technique for studying flow within engineering equipment. *Nucl. Instrum. Methods Phys. Res. Sect. A* **1993**, *326*, 592–607. [CrossRef]
77. Leadbeater, T.W. The Development of Positron Imaging Systems for Applications in Industrial Process Tomography. Ph.D. Thesis, The University of Birmingham, Birmingham, UK, 2009.
78. Leadbeater, T.W.; Parker, D.J.; Gargiuli, J. Positron imaging systems for studying particulate, granular and multiphase flows. *Particuology* **2012**, *10*, 146–153. [CrossRef]
79. Cole, K.; Buffler, A.; Cilliers, J.J.; Govender, I.; Heng, J.Y.Y.; Liu, C.; Parker, D.J.; Shah, U.V.; van Heerden, M.; Fan, X. A surface coating method to modify tracers for positron emission particle tracking (PEPT) measurements of froth flotation. *Powder Technol.* **2014**, *263*, 26–30. [CrossRef]
80. Lin, J.S.; Chen, M.M.; Chao, B.T. A novel radioactive particle tracking facility for measurement of solids motion in gas fluidized beds. *AIChE J.* **1985**, *31*, 465–473. [CrossRef]
81. Van de Velden, M.; Baeyens, J.; Seville, J.P.K.; Fan, X. The solids flow in the riser of a Circulating Fluidised Bed (CFB) viewed by Positron Emission Particle Tracking (PEPT). *Powder Technol.* **2008**, *183*, 290–296. [CrossRef]
82. van Buijtenen, M.S.; van Dijk, W.-J.; Deen, N.G.; Kuipers, J.A.M.; Leadbeater, T.; Parker, D.J. Numerical and experimental study on multiple-spout fluidized beds. *Chem. Eng. Sci.* **2011**, *66*, 2368–2376. [CrossRef]
83. Laverman, J.A.; Fan, X.; Ingram, A.; Annaland, M.v.S.; Parker, D.J.; Seville, J.P.K.; Kuipers, J.A.M. Experimental study on the influence of bed material on the scaling of solids circulation patterns in 3D bubbling gas–solid fluidized beds of glass and polyethylene using positron emission particle tracking. *Powder Technol.* **2012**, *224*, 297–305. [CrossRef]
84. Hensler, T.; Tupy, M.; Strer, T.; Pöschel, T.; Wirth, K.-E. Positron emission particle tracking in fluidized beds with secondary gas injection. *Powder Technol.* **2015**, *279*, 113–122. [CrossRef]
85. Xu, Y.; Li, T.; Lu, L.; Tebianian, S.; Chaouki, J.; Leadbeater, T.W.; Jafari, R.; Parker, D.J.; Seville, J.; Ellis, N.; et al. Numerical and experimental comparison of tracer particle and averaging techniques for particle velocities in a fluidized bed. *Chem. Eng. Sci.* **2019**, *195*, 356–366. [CrossRef]
86. Windows-Yule, C.R.K.; Gibson, S.; Werner, D.; Parker, D.J.; Kokalova, T.Z.; Seville, J.P.K. Effect of distributor design on particle distribution in a binary fluidised bed. *Powder Technol.* **2020**, *367*, 1–9. [CrossRef]
87. Xu, Y.; Li, T.; Lu, L.; Gao, X.; Tebianian, S.; Grace, J.R.; Chaouki, J.; Leadbeater, T.W.; Jafari, R.; Parker, D.J.; et al. Development and confirmation of a simple procedure to measure solids distribution in fluidized beds using tracer particles. *Chem. Eng. Sci.* **2020**, *217*, 115501. [CrossRef]
88. Adnan, M.; Sun, J.; Ahmad, N.; Wei, J.J. Validation and sensitivity analysis of an Eulerian-Eulerian two-fluid model (TFM) for 3D simulations of a tapered fluidized bed. *Powder Technol.* **2022**, *396*, 490–518. [CrossRef]

89. Jayasundara, C.T.; Yang, R.Y.; Guo, B.Y.; Yu, A.B.; Govender, I.; Mainza, A.; Westhuizen, A.v.d.; Rubenstein, J. CFD–DEM modelling of particle flow in IsaMills—Comparison between simulations and PEPT measurements. *Miner. Eng.* **2011**, *24*, 181–187. [CrossRef]
90. Böttcher, A.-C.; Schilde, C.; Kwade, A. Experimental assessment of grinding bead velocity distributions and stressing conditions in stirred media mills. *Adv. Powder Technol.* **2021**, *32*, 413–423. [CrossRef]
91. Morrison, A.J.; Govender, I.; Mainza, A.N.; Parker, D.J. The shape and behaviour of a granular bed in a rotating drum using Eulerian flow fields obtained from PEPT. *Chem. Eng. Sci.* **2016**, *152*, 186–198. [CrossRef]
92. de Klerk, D.N.; Govender, I.; Mainza, A.N. Geometric features of tumbling mill flows: A positron emission particle tracking investigation. *Chem. Eng. Sci.* **2019**, *206*, 41–49. [CrossRef]
93. Herald, M.T.; Sykes, J.A.; Werner, D.; Seville, J.P.K.; Windows-Yule, C.R.K. DEM2GATE: Combining discrete element method simulation with virtual positron emission particle tracking experiments. *Powder Technol.* **2022**, *401*, 117302. [CrossRef]
94. Cole, K.; Brito-Parada, P.R.; Hadler, K.; Mesa, D.; Neethling, S.J.; Norori-McCormac, A.M.; Cilliers, J.J. Characterisation of solid hydrodynamics in a three-phase stirred tank reactor with positron emission particle tracking (PEPT). *Chem. Eng. J.* **2022**, *433*, 133819. [CrossRef]
95. Sheikh, H.A.; Savari, C.; Barigou, M. Lagrangian stochastic modelling of liquid flow in a mechanically agitated vessel. *Chem. Eng. Sci.* **2022**, *249*, 117318. [CrossRef]
96. Savari, C.; Li, K.; Barigou, M. Multiscale wavelet analysis of 3D Lagrangian trajectories in a mechanically agitated vessel. *Chem. Eng. Sci.* **2022**, *260*, 117844. [CrossRef]
97. Li, K.; Savari, C.; Barigou, M. Computation of Lagrangian coherent structures from experimental fluid trajectory measurements in a mechanically agitated vessel. *Chem. Eng. Sci.* **2022**, *254*, 117598. [CrossRef]
98. Radman, J.R.; Langlois, R.; Leadbeater, T.; Finch, J.; Rowson, N.; Waters, K. Particle flow visualization in quartz slurry inside a hydrocyclone using the positron emission particle tracking technique. *Miner. Eng.* **2014**, *62*, 142–145. [CrossRef]
99. Sovechles, J.M.; Boucher, D.; Pax, R.; Leadbeater, T.; Sasmito, A.P.; Waters, K.E. Performance analysis of a new positron camera geometry for high speed, fine particle tracking. *Meas. Sci. Technol.* **2017**, *28*, 095402. [CrossRef]
100. Hoffmann, A.C.; Skorpen, Å.; Chang, Y.-F. Positron emission particle tracking and CFD investigation of hydrocyclones acting on liquids of varying viscosity. *Chem. Eng. Sci.* **2019**, *200*, 310–319. [CrossRef]
101. Boucher, D.; Deng, Z.; Leadbeater, T.W.; Langlois, R.; Waters, K.E. Speed analysis of quartz and hematite particles in a spiral concentrator by PEPT. *Miner. Eng.* **2016**, *91*, 86–91. [CrossRef]
102. Boucher, D.; Deng, Z.; Leadbeater, T.; Langlois, R.; Waters, K.E. Observation of iron ore beneficiation within a spiral concentrator by positron emission particle tracking of large (Ø = 1440 μm) and small (Ø = 58 μm) hematite and quartz tracers. *Chem. Eng. Sci.* **2016**, *140*, 217–232. [CrossRef]
103. Boucher, D.; Jordens, A.; Sovechles, J.; Langlois, R.; Leadbeater, T.W.; Rowson, N.A.; Cilliers, J.J.; Waters, K.E. Direct mineral tracer activation in positron emission particle tracking of a flotation cell. *Miner. Eng.* **2017**, *100*, 155–165. [CrossRef]
104. Cole, K.; Brito-Parada, P.R.; Morrison, A.; Govender, I.; Buffler, A.; Hadler, K.; Cilliers, J.J. Using positron emission tomography (PET) to determine liquid content in overflowing foam. *Chem. Eng. Res. Des.* **2015**, *94*, 721–725. [CrossRef]
105. Waters, K.E.; Rowson, N.A.; Fan, X.; Cilliers, J.J. Following the path of hydrophobic and hydrophilic particles in a Denver Cell using positron emission particle tracking. *Asia-Pac. J. Chem. Eng.* **2009**, *4*, 218–225. [CrossRef]
106. Waters, K.E.; Rowson, N.A.; Fan, X.F.; Parker, D.J.; Cilliers, J.J. The use of positron emission particle tracking as a method for tracking particles in flotation froths. *Philos. Mag. Lett.* **2008**, *88*, 735–739. [CrossRef]
107. Waters, K.E.; Rowson, N.A.; Fan, X.; Parker, D.J.; Cilliers, J.J. Positron emission particle tracking as a method to map the movement of particles in the pulp and froth phases. *Miner. Eng.* **2008**, *21*, 877–882. [CrossRef]
108. Sommer, A.E.; Ortmann, K.; Van Heerden, M.; Richter, T.; Leadbeater, T.; Cole, K.; Heitkam, S.; Brito-Parada, P.R.; Eckert, K. Application of Positron Emission Particle Tracking (PEPT) to measure the bubble-particle interaction in a turbulent and dense flow. *Miner. Eng.* **2020**, *156*, 106410. [CrossRef]
109. Mesa, D.; Cole, K.; van Heerden, M.R.; Brito-Parada, P.R. Hydrodynamic characterisation of flotation impeller designs using Positron Emission Particle Tracking (PEPT). *Sep. Purif. Technol.* **2021**, *276*, 119316. [CrossRef]
110. Cole, K.; Barker, D.J.; Brito-Parada, P.R.; Buffler, A.; Hadler, K.; Mackay, I.; Mesa, D.; Morrison, A.J.; Neethling, S.; Norori-McCormac, A.; et al. Standard method for performing positron emission particle tracking (PEPT) measurements of froth flotation at PEPT Cape Town. *MethodsX* **2022**, *9*, 101680. [CrossRef]
111. Mesa, D.; van Heerden, M.; Cole, K.; Neethling, S.J.; Brito-Parada, P.R. Hydrodynamics in a three-phase flotation system—Fluid following with a new hydrogel tracer for Positron Emission Particle Tracking (PEPT). *Chem. Eng. Sci.* **2022**, *260*, 117842. [CrossRef]
112. Geldart, D. The effect of particle size and size distribution on the behaviour of gas-fluidised beds. *Powder Technol.* **1972**, *6*, 201–215. [CrossRef]
113. Geldart, D. Types of gas fluidization. *Powder Technol.* **1973**, *7*, 285–292. [CrossRef]
114. Grace, J.R. Contacting modes and behaviour classification of gas—Solid and other two-phase suspensions. *Can. J. Chem. Eng.* **1986**, *64*, 353–363. [CrossRef]
115. Parker, D.J.; Forster, R.N.; Fowles, P.; Takhar, P.S. Positron emission particle tracking using the new Birmingham positron camera. *Nucl. Instrum. Methods Phys. Res. Sect. A* **2002**, *477*, 540–545. [CrossRef]

116. Boucher, D.; Gharib, N.; Deng, Z.; Leadbeater, T.; Langlois, R.; Waters, K.E. PEPT Validation of a CFD-DEM Model of a Fine Quartz Particle (60 µm) Behaviour in Stirred Water. *Procedia Eng.* **2015**, *102*, 1305–1315. [CrossRef]
117. Oshitani, J.; Trisakti, B.; Tanaka, Z. Evaluation of fluidized particle flow by measurement of apparent buoyancy. *Adv. Powder Technol.* **2001**, *12*, 95–104. [CrossRef]
118. Leadbeater, T.W.; Seville, J.P.K.; Parker, D.J. On trajectory and velocity measurements in fluidized beds using positron emission particle tracking (PEPT). *Can. J. Chem. Eng.* **2023**, *101*, 269–282. [CrossRef]